This article has been accepted for publication in a future issue of this journal, but has not been fully edited. Content may change prior to final publication.
Citation information: DOI: 10.1109/tase.2026.3653716, IEEE Transactions on Automation Science and Engineering

Distributionally Robust Chance-Constrained Unit Commitment for Power Systems Considering Wind Power Curtailment and Load Shedding Levels

Min Du, *Member, IEEE*, Xin Zhang, *Senior Member, IEEE*, Jinning Zhang, *Member, IEEE*, Zidong Wang, *Fellow, IEEE*, Vladimir Terzija, *Fellow, IEEE*

***Abstract*—With increasing wind power penetration, the inherent uncertainty of wind power poses significant challenges to dispatch decisions in power systems. To address this issue, this paper proposes a two-stage distributionally robust chance-constrained (TDRC) model for the unit commitment problem with wind power uncertainty. In this model, an ambiguity confidence set is developed to characterise wind power uncertainty with unknown probability distributions, and wind power curtailment and load shedding levels are modelled as chance constraints to balance wind power uncertainty and system security of dispatch decisions. A hybrid parallel solution (HPS) is proposed for efficient computation by integrating Benders decomposition (BD) and column-and-constraint generation (C&CG) methods. Case studies on the IEEE 24- and 118-bus systems demonstrate the rationality of the proposed approach, while experiments on a practical 126-bus system using the cyber-physical power system (CPPS) dispatch platform further validate the effectiveness and practical applicability of the proposed TDRC model.**

***Note to Practitioners*—This paper addresses the unit commitment problem in power systems with uncertain wind power by developing a two-stage distributionally robust chance-constrained (TDRC) model. This model captures the worst-case probability distribution of wind power output within an ambiguity confidence set that is designed based on L_1 and L_∞ norms. This ensures that the dispatch decisions can handle extreme scenarios in wind power output, thereby improving the reliability of the system. Meanwhile, chance constraints are employed to regulate wind power curtailment and load shedding levels, balancing the flexibility and conservativeness in dispatch decision-making. Finally, a hybrid parallel solution (HPS) algorithm is developed to solve the TDRC model, innovatively integrating Benders decomposition (BD) and column-and-constraint generation (C&CG) methods to improve computational efficiency. The proposed TDRC framework can be implemented for security dispatch of practical large-scale power systems with uncertain wind power.**

***Index Terms*— Ambiguity confidence set, power systems, wind power curtailment, load shedding, hybrid parallel solution algorithm.**

This work was supported by the U.K. Research and Innovation Future Leaders Fellowship entitled 'Digitalisation of Electrical Power and Energy Systems Operation' under Grant MR/W011360/2. (*Corresponding author: Xin Zhang*.)

Min Du and Xin Zhang are with the School of Electrical and Electronic Engineering, University of Sheffield, Sheffield, S10 2TN United Kingdom (e-mail: m.du@sheffield.ac.uk; xin.zhang1@sheffield.ac.uk).

Jinning Zhang is with the School of Engineering, University of Leicester, Leicester, LE1 7RH United Kingdom (e-mail: jz388@leicester.ac.uk).

Zidong Wang is with the Department of Computer Science, Brunel University London, UB8 3PH Uxbridge United Kingdom (e-mail: zidong.wang@brunel.ac.uk).

Vladimir Terzija is with the School of Engineering, Merz Court E4.41, Newcastle University, Newcastle upon Tyne NE1 7RU United Kingdom (e-mail: vladimir.terzija@newcastle.ac.uk).

NOMENCLATURE

Constants and Parameters

NT	Number of time periods in 24 h.
i, d, w, t	Indices of units, loads, wind farms, and time periods.
$\mathcal{D}$	Confidence set for wind power output probability distribution.
NG, ND, NW	Numbers of units, loads, and wind farms.
s	Index of wind power output scenarios.
p_s^0	Initial probability value.
β_w	Wind power utilisation rate.
T_i^{on}, T_i^{off}	Minimum ON and OFF time of unit i.
$X_{i,t}^{\text{on}}$, $X_{i,t}^{\text{off}}$	ON and OFF time of unit i at time t.
C_i^g	Generation cost of unit i.
C_i^{up}, C_i^{dw}	Upward and downward reserve costs of unit i.
S_i^{up}, S_i^{dw}	Startup and shutdown costs of unit i.
$\overline{r}_i^{up}$, $\overline{r}_i^{dw}$	Maximum upward and downward reserve of unit i.
$\overline{P}_i^g$, $\underline{P}_i^g$	Upper and lower bounds of generation of unit i.
$\overline{r}_t^{dw}$, $\underline{r}_t^{dw}$	Upper and lower bounds of downward reserve of units at time t.
$\overline{r}_t^{up}$, $\underline{r}_t^{up}$	Upper and lower bounds of upward reserve of units at time t.
SF	Shift factor matrix.
KP, **KD**, **KW**	Bus-unit, bus-load, and bus-wind farm incidence matrices.
$\overline{\boldsymbol{f}}$	Power flow limit vector of lines.
$P_{d,t}^d$, $\boldsymbol{P}_t^d$	Load demand and load demand vector of load buses at time t.
$\overline{P}_{w,t}^w$	Forecasted power output of wind farm w at time t.
$P_{w,t}^{w,0}(s)$	Power output scenario s of wind farm w at time t.
γ_{LSL}	Load shedding level (LSL) limitation.

γ_{WPCL}	Wind power curtailment level (WPCL) limitation.
μ	Power flow capacity expansion factor.
Variables	
p_s	Probability of wind power output scenario s.
$P_{i,t}^{g}$	Generation of unit i at time t.
$\Delta P_{w,t}^{w}(s)$	Power curtailment of wind farm w at time t in wind power output scenario s.
$I_{i,t}$, $y_{i,t}$, $z_{i,t}$	Binary commitment, startup, and shutdown variables of unit i at time t.
$r_{i,t}^{up}$, $r_{i,t}^{dw}$	Upward and downward reserve of unit i at time t.
$P_{w,t}^{w}$	Power output of wind farm w at time t.
$r_{i,t}^{up'}(s)$, $r_{i,t}^{dw'}(s)$	Upward and downward reserve provided by unit i at time t in wind power output scenario s.
$\Delta P_{d,t}^{d}(s)$	Load shedding of load bus d at time t in wind power output scenario s.
$\boldsymbol{P}_t^{g}$	Generation vector of units at time t.
$\boldsymbol{P}_t^{w}$	Power output vector of wind farms at time t.
$\boldsymbol{f}^{t}$	Power flow vector of lines at time t.
$\boldsymbol{P}_t^{G}(s)$	Generation vector of units at time t in wind power output scenario s.
$\Delta\boldsymbol{P}_t^{w}(s)$	Power curtailment vector of wind farms at time t in wind power output scenario s.
$\Delta\boldsymbol{P}_t^{d}(s)$	Load shedding vector of load buses at time t in wind power output scenario s.
$\boldsymbol{F}^{t}(s)$	Power flow vector of lines at time t in wind power output scenario s.

I. Introduction

OVER the last several decades, environmental issues and energy crises have promoted the sustainable development of renewable energy, such as wind power [1-3]. For example, Uruguay, Ireland, and the United Kingdom now generate 40.4%, 38.0%, and 35.5% of their electricity from wind power, respectively [4]. However, high wind power penetration also poses a security risk to power system operation as it may compromise dispatch decisions due to its inherent uncertainty [5, 6]. Thus, it is crucial for the system operator to utilise Supervisory Control and Data Acquisition (SCADA) system and energy management system (EMS) to manage wind power uncertainty in order to make robust dispatch decisions, such as economic dispatch [7, 8] and unit commitment [9, 10].

In practice, day-ahead unit commitment and economic dispatch aim to minimise the operational cost of power systems by considering uncertain wind power, while enhancing the reliability of the system based on dispatch decisions [11]. At present, several advanced modelling methods are employed to deal with uncertain wind power. For example, stochastic programming (SP) (e.g., [12, 13]) and robust optimisation (RO) (e.g., [14, 15]) techniques are widely utilised to address wind power uncertainty and determine robust dispatch decisions. Here, the SP approach characterises the uncertainty of wind power output by generating a set of representative scenarios derived from an assumed probability distribution of wind power. Nevertheless, since the true distribution of wind power output is often unknown, a large number of scenarios must be constructed to sufficiently capture the underlying stochastic behaviour, which inevitably results in a significant computational burden. In contrast, a RO approach characterises uncertainty through an ambiguity set that encompasses all possible realisations of uncertain parameters, without relying on a specific probability distribution. However, this method often yields overly conservative dispatch decisions, as it focuses on the worst-case realisation of uncertainty, which is typically of low probability or even unrealistic under practical power system operating conditions.

To address these issues in SP and RO methods, the authors in [16, 17] proposed a distributionally robust optimisation (DRO) approach for power systems against uncertainties. The DRO method considered uncertainty in the probability distributions of uncertain variables, thereby making more appropriate dispatch decisions. Thus, a moment-based DRO method was developed in [18] for the system operator to determine the optimal dispatch decisions that can hedge against uncertain variables in the unit commitment problem. However, incorporating second-order moment information introduces nonlinear constraints, thereby complicating the reformulation of the problem into a convex optimisation framework. Moreover, this moment-based method only captures a portion of the true distribution by considering merely the first and second moments, which may still degrade the reliability and economic efficiency of dispatch decisions. Then, the authors in [19] proposed a statistical-distance-based DRO approach to comprehensively quantify the discrepancy between probability distributions of uncertainty. Compared with previous DRO methods, this statistical-distance-based approach addresses uncertain variables by incorporating more detailed information about their probability distributions. Similarly, the authors in [20] presented a Kullback-Leibler (KL) divergence-based DRO methodology to address the uncertainty of wind power in the unit commitment problem for power systems. However, this approach applies only to continuous distributions with well-defined probability densities. Moreover, when the wind power output exhibits a heavy-tailed distribution, the KL-based DRO formulation may yield an unbounded or infinite worst-case expectation, which undermines its practical applicability. To deal with the drawbacks of this method, a Wasserstein metric-based DRO approach was further developed to tackle the unit commitment problem in power systems under uncertainty [21]. However, both continuous and discrete Wasserstein metric-based DRO methods still present some disadvantages. Specifically, the continuous Wasserstein metric-based DRO method involves nonlinear functional constraints on probability distributions of uncertain variables, leading to high computational complexity. In the discrete Wasserstein-distance-based DRO model, the support points are treated as decision variables, which introduces nonlinearities and makes the optimisation problem nonconvex. In addition, its performance depends heavily on the sample size, as too few samples may cause overfitting, while too many samples can impose excessive computational burdens. Then, the authors in [22] presented a data-driven DRO method for the unit

commitment problem in power systems with uncertain variables, which employed a norm (e.g., L_1 norm or L_∞ norm) to construct a confidence set that covers the probability distribution of uncertain variables. The norm-based DRO method neither requires moment information nor relies on probability density assumptions, and it does not introduce nonlinear terms, thereby achieving a better trade-off between the economic efficiency and robustness of dispatch decisions in large-scale power systems.

In addition, chance-constrained optimisation (CO) method is an effective approach for solving the unit commitment problem with uncertain variables [23]. At present, researchers have extensively studied the distributionally robust chance-constrained optimisation (DRCO) approach [24, 25]. For example, a data-driven DRCO model [26] was applied to tackle the unit commitment problem for power systems with uncertain wind power, allowing power imbalances at a low probability level predefined by a chance-constrained approach. In [27], the authors proposed a chance-constrained method for energy management involving uncertain wind power, integrated with the DRO method, in which the power balance constraints were formulated in a probabilistic manner. Recently, a joint chance-constrained model based on the DRO approach was developed in [28] for microgrids considering power system contingencies and uncertain wind power. However, high wind power utilisation and low wind power curtailment are often excluded from the optimisation approach in these methods, leading to unsustainable dispatch decisions when wind power utilisation is encouraged under practical power system operating conditions.

To support the utilisation of renewable energy, wind power is often prioritised by system operators in dispatch decisions, and wind power curtailment are therefore reduced, as is the case in Germany [29]. By incorporating wind power curtailment levels into dispatch decisions, the system operator can optimise the dispatch of available renewable energy, thereby reducing the amount of wind power that is curtailed unnecessarily. This leads to higher wind power utilisation, which is particularly beneficial in power systems with high renewable energy penetration. In addition, uncertain wind power may cause power imbalances that can result in large-scale load shedding, which poses a significant threat to system security [30]. By considering load shedding levels, the system operator can establish acceptable levels of load shedding risk while still ensuring that the overall system remains reliable even under uncertain wind power output. Overall, from a practical power system operation perspective, the system operator should proactively consider wind power curtailment and load shedding levels, balancing the wind power uncertainty and system security in dispatch decisions.

TABLE I.
COMPARISON OF REPRESENTATIVE LITERATURE WITH THE PROPOSED METHOD

Ref.	Category	Uncertainty handling methods	Chance-constrained	Unit commitment	Wind power curtailment level	Load shedding level	Solution algorithms	Dispatch Platforms
[12]	SP	Multiple scenarios	×	✓	×	×	BD	×
[14]	RO	Worst-case scenario	×	✓	×	×	C&CG	×
[18]	Moment-based DRO	First- and second order	✓	✓	×	×	BD	×
[20]	KL-based DRO	KL divergence	×	✓	×	×	C&CG	×
[21]	Wasserstein-based DRO	Wasserstein metric	×	✓	×	×	C&CG	×
[22]	Data-driven DRO	Confidence set	×	✓	×	×	BD	×
[24]	Wasserstein-based DRO	Wasserstein metric	✓	×	×	×	C&CG	×
[26]	Data-driven DRO	Ambiguity set	✓	✓	×	×	C&CG	×
This paper	Norm-based DRO	Combined L_1 and L_∞ -norms	✓	✓	✓	✓	BD+C&CG	✓

† This paper integrates the BD and C&CG methods into a hybrid parallel solution (HPS) algorithm, denoted as BD+C&CG.

In summary, Table I presents a comparison between the proposed approach and several representative studies in the literature. Existing studies reveal the following research gaps: SP approaches depend on large amounts of historical data to generate representative scenarios, while RO approaches often yield overly conservative dispatch decisions. Although DRO approaches are developed to deal with wind power uncertainty, most studies ignore wind power curtailment and load shedding levels under practical power system operating conditions, and these conditions are not incorporated into chance constraints to adjust risk-averse levels for wind power uncertainty and system security in decision-making in unit commitment. Furthermore, few studies have developed scalable solution algorithms to improve computational efficiency or have validated their respective proposed methods through the practical power system dispatch platform for large-scale systems. To address these research gaps, this paper proposes a two-stage distributionally robust chance-constrained (TDRC) model that explicitly considers wind power curtailment and load shedding levels, solved via integrated BD and C&CG methods. The main contributions of this paper are summarised below:

(1) A two-stage distributionally robust chance-constrained (TDRC) model is proposed for the unit commitment problem with uncertain wind power. The TDRC model incorporates chance constraints to flexibly regulate wind power curtailment and load shedding levels by constructing an ambiguity set based on L_1 and L_∞ norms to characterise the uncertainty of wind power output. These features enable the model to achieve the trade-off between the wind power uncertainty and system security of dispatch decisions.

(2) To solve the TDRC model, probability theory is first used to transform chance constraints into equivalent deterministic constraints, reformulating the problem into a tractable formulation. Then, a hybrid parallel solution (HPS) algorithm is developed to iteratively solve the TDRC model through a decomposition into a master and multiple sub-problems. The proposed algorithm integrates the advantages of BD and C&CG methods to

improve computational efficiency and does not rely on duality information.

(3) Extensive case studies are conducted through both numerical simulations and a cyber-physical power system (CPPS) dispatch platform to verify the validity and rationality of the proposed approach. The numerical studies demonstrate the superior robustness and computational efficiency of the TDRC model and the HPS algorithm, while the SCADA and EMS integrated CPPS dispatch platform further validates the practical applicability of the proposed model under realistic operational conditions.

The remainder of this paper is organised as follows: Section II gives the mathematical formulation and overall framework of the TDRC model. Section III presents the linearisation of the nonlinear constraints and develops a HPS algorithm to efficiently solve the TDRC model. Section IV conducts case studies on the IEEE 24- and 118-bus systems and experiments on a practical 126-bus system using the CPPS dispatch platform. Section V concludes this paper and discusses potential directions for future research.

II. Mathematical Formulation

A. Ambiguity Confidence Set

In fact, achieving an accurate probability distribution of wind power output is not feasible for the system operator. Thus, the L_1 norm and the L_∞ norm are used to construct an ambiguity confidence set to model wind power uncertainty, described as follows:

$$\mathcal{D}=\left\{\boldsymbol{p}\left|\begin{array}{l}\sum_{s=1}^{K}p_s=1\\ p_s\in[0,1]\quad s=1,\ldots,K\\ \mathcal{D}_1=\left\{\boldsymbol{p}\in\mathbb{R}^K\left|\left\|\boldsymbol{p}-\boldsymbol{p}^0\right\|_1\le\theta\right.\right\}\\ =\left\{\boldsymbol{p}\in\mathbb{R}^K\left|\sum_{s=1}^{K}\left|p_s-p_s^0\right|\le\theta\right.\right\}\\ \mathcal{D}_\infty=\left\{\boldsymbol{p}\in\mathbb{R}^K\left|\left\|\boldsymbol{p}-\boldsymbol{p}^0\right\|_\infty\le\theta\right.\right\}\\ =\left\{\boldsymbol{p}\in\mathbb{R}^K\left|\max_{1\le s\le K}\left|p_s-p_s^0\right|\le\theta\right.\right\}\end{array}\right.\right\} \tag{1}$$

where θ is a scalar parameter. According to [31], the following relationships are obtained:

$$\Pr\left\{\sum_{s=1}^{K}\left|p_s-p_s^0\right|\le\theta\right\}\ge 1-2Ke^{-2N_s\theta/K} \tag{2}$$

$$\Pr\left\{\max_{1\le s\le K}\left|p_s-p_s^0\right|\le\theta\right\}\ge 1-2Ke^{-2N_s\theta} \tag{3}$$

where K denotes the number of clusters, and N_s denotes the data sample sizes. The right-hand side of constraints (2) and (3), denoted by α, represent the confidence level. Thus, the following relationships are obtained:

$$\theta_1=\frac{K}{2N_s}\ln\frac{2K}{1-\alpha} \tag{4}$$

$$\theta_\infty=\frac{1}{2N_s}\ln\frac{2K}{1-\alpha} \tag{5}$$

Fig. 1 illustrates the relationship between wind power uncertainty and its ambiguity set. The ambiguity set is designed to capture more possible probability distributions. The worst-case probability distribution is identified within the ambiguity confidence set to determine robust dispatch decisions.

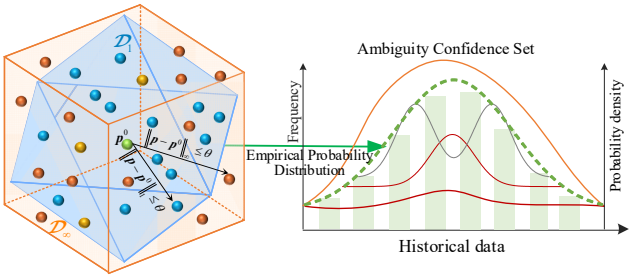

Fig. 1. Illustration of the ambiguity confidence set.

B. Proposed TDRC Model

In this section, a two-stage distributionally robust optimisation model is developed with chance constraints based on an ambiguity confidence set $\mathcal{D}$, aiming to regulate wind power curtailment and load shedding levels under the worst-case probability distribution. Specifically, the first-stage objective is to minimise the total cost of optimal unit dispatch, which comprises unit generation costs, startup and shutdown costs, upward and downward reserve costs, and the expected penalty cost from the second-stage due to wind power curtailment and load shedding under the worst-case probability distribution. The second-stage is essentially a bilevel max-min problem that considers wind power uncertainty in power systems. The upper-level problem identifies the worst-case probability distribution within $\mathcal{D}$, while the lower-level problem minimises the penalty cost associated with wind power curtailment and load shedding under the worst-case probability distribution. The overall structure of the TDRC framework is illustrated in Fig. 2.

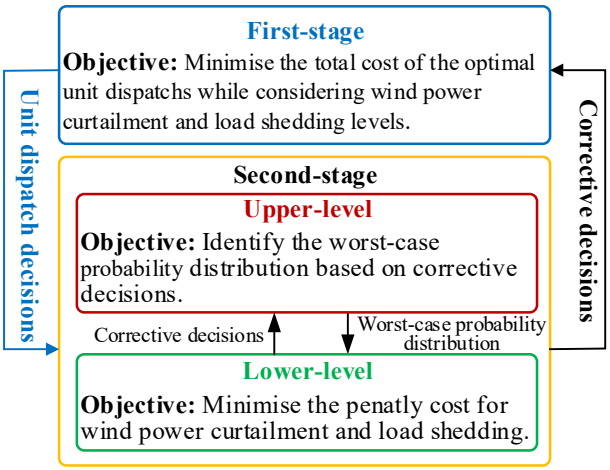

Fig. 2. Framework of the two-stage distributionally robust chance-constrained model.

1) First-stage of the TDRC model: The first-stage of the TDRC model is to minimise the total cost and optimise the unit dispatch decisions to ensure acceptable levels of wind power

curtailment and load shedding. Thus, the first-stage model is formulated below:

$$\min \sum_{t=1}^{\mathrm{NT}} \sum_{i=1}^{\mathrm{NG}} \left(C_i^g P_{i,t}^g + S_i^{up} y_{i,t} + S_i^{dw} z_{i,t} + C_i^{up} r_{i,t}^{up} + C_i^{dw} r_{i,t}^{dw} \right) \quad (6)$$

subject to:

$$y_{i,t} + z_{i,t} \le 1 \qquad \forall i, \forall t \quad (7)$$

$$y_{i,t} - z_{i,t} = I_{i,t} - I_{i,(t-1)} \qquad \forall i, \forall t \quad (8)$$

$$\left[X_{i,(t-1)}^{\mathrm{on}} - T_i^{\mathrm{on}} \right] \left[I_{i,(t-1)} - I_{i,t} \right] \ge 0 \qquad \forall i, \forall t \quad (9)$$

$$\left[X_{i,(t-1)}^{\mathrm{off}} - T_i^{\mathrm{off}} \right] \left[I_{i,t} - I_{i,(t-1)} \right] \ge 0 \qquad \forall i, \forall t \quad (10)$$

$$\sum_{i=1}^{\mathrm{NG}} P_{i,t}^g + \sum_{w=1}^{\mathrm{NW}} \overline{P}_{w,t}^w = \sum_{d=1}^{\mathrm{ND}} P_{d,t}^d \qquad \forall t \quad (11)$$

$$P_{i,t}^g + r_{i,t}^{up} \le \overline{P}_i^g I_{i,t} \qquad \forall i, \forall t \quad (12)$$

$$P_{i,t}^g - r_{i,t}^{dw} \ge \underline{P}_i^g I_{i,t} \qquad \forall i, \forall t \quad (13)$$

$$0 \le r_{i,t}^{up} \le \overline{r}_i^{up} I_{i,t} \qquad \forall i, \forall t \quad (14)$$

$$0 \le r_{i,t}^{dw} \le \overline{r}_i^{dw} I_{i,t} \qquad \forall i, \forall t \quad (15)$$

$$\underline{r}_t^{up} \le \sum_{i=1}^{\mathrm{NG}} r_{i,t}^{up} \le \overline{r}_t^{up} \qquad \forall i, \forall t \quad (16)$$

$$\underline{r}_t^{dw} \le \sum_{i=1}^{\mathrm{NG}} r_{i,t}^{dw} \le \overline{r}_t^{dw} \qquad \forall i, \forall t \quad (17)$$

$$0 \le P_{w,t}^w \le \overline{P}_{w,t}^w \qquad \forall w, \forall t \quad (18)$$

$$\mathbf{SF} \cdot \left(\mathbf{KP} \cdot \boldsymbol{P}_t^g + \mathbf{KW} \cdot \boldsymbol{P}_t^w - \mathbf{KD} \cdot \boldsymbol{P}_t^d \right) = \boldsymbol{f}^t \quad \forall t \quad (19)$$

$$-\overline{\boldsymbol{f}} \le \boldsymbol{f}^t \le \overline{\boldsymbol{f}} \qquad \forall t \quad (20)$$

$$\Pr\left\{ \sum_{d=1}^{\mathrm{ND}} P_{d,t}^d \le \sum_{i=1}^{\mathrm{NG}} P_{i,t}^g + \sum_{w=1}^{\mathrm{NW}} P_{w,t}^{w,0}(s) + \sum_{i=1}^{\mathrm{NG}} r_{i,t}^{up} \right\} \ge 1 - \gamma_{\mathrm{LSL}} \qquad \forall t \quad (21)$$

$$\Pr\left\{ \beta_w \sum_{w=1}^{\mathrm{NW}} P_{w,t}^{w,0}(s) + \sum_{i=1}^{\mathrm{NG}} P_{i,t}^g - \sum_{i=1}^{\mathrm{NG}} r_{i,t}^{dw} \le \sum_{i=1}^{\mathrm{ND}} P_{d,t}^d \right\} \ge 1 - \gamma_{\mathrm{WPCL}} \qquad \forall t \quad (22)$$

$$I_{i,t}, y_{i,t}, z_{i,t} \in \{0,1\} \qquad \forall i, \forall t \quad (23)$$

where objective (6) aims to minimise the total unit dispatch cost including the unit generation costs, startup and shutdown costs, and upward and downward reserve costs, thereby defining the first-stage optimal dispatch decisions objective of the TDRC model. Constraints (7) and (8) represent the startup and shutdown unit commitment status constraints for each unit, respectively. Constraints (9) and (10) limit the minimum on- and off-time of each unit, respectively. Constraint (11) represents the power balance equation. Constraints (12) and (13) represent the minimum and maximum generation capability limitations for each unit, respectively. Constraints (14) and (15) define the up and downward reserve capability constraints for each unit, respectively. Constraints (16) and (17) represent the up and downward reserve capability constraints for the entire system, respectively. Constraint (18) indicates the actual wind power output limitation. Constraint (19) calculates the power flow, and constraint (20) restricts this power flow. Constraints (21) and (22) are chance constraints associated with load shedding and wind power curtailment levels, respectively.

More specifically, constraint (21) ensures that the available generation, wind power, and upward reserve are sufficient to meet the total demand with a probability no less than $1-\gamma_{\mathrm{LSL}}$, thereby limiting the load shedding level. Constraint (22) limits the probability of excessive wind power curtailment by ensuring that the available downward reserve and generation flexibility are sufficient to keep the curtailed wind power within its allowable range with a probability not lower than $1-\gamma_{\mathrm{WPCL}}$. Also, constraint (23) defines the binary commitment variables $I_{i,t}$, $y_{i,t}$ and $z_{i,t}$, which represent on and off, startup, and shutdown states of each unit.

2) Second-stage of the TDRC model: The second-stage of the TDRC model aims to minimise the expected penalty cost incurred under the worst-case probability distribution. Thus, the second-stage model is expressed as follows:

$$\max_{p_s \in \mathcal{D}} \sum_{s=1}^{K} p_s \cdot \min \left[\sum_{t=1}^{\mathrm{NT}} \left(\sum_{w=1}^{\mathrm{NW}} C_w \Delta P_{w,t}^w(s) + \sum_{d=1}^{\mathrm{ND}} C_d \Delta P_{d,t}^d(s) \right) \right] \quad (24)$$

subject to:

$$P_{i,t}^G(s) = P_{i,t}^g + r_{i,t}^{up'}(s) - r_{i,t}^{dw'}(s) \qquad \forall i, \forall t, \forall s \quad (25)$$

$$\sum_{d=1}^{\mathrm{ND}} \left(P_{d,t}^d - \Delta P_{d,t}^d(s) \right) = \sum_{i=1}^{\mathrm{NG}} P_{i,t}^G(s) + \sum_{w=1}^{\mathrm{NW}} \left(P_{i,t}^{w,0}(s) - \Delta P_{w,t}^w(s) \right) \qquad \forall i, \forall t, \forall s \quad (26)$$

$$\underline{P}_i^g I_{i,t} \le P_{i,t}^G(s) \le \overline{P}_i^g I_{i,t} \qquad \forall i, \forall t, \forall s \quad (27)$$

$$0 \le r_{i,t}^{up'}(s) \le r_{i,t}^{up} \qquad \forall i, \forall t, \forall s \quad (28)$$

$$0 \le r_{i,t}^{dw'}(s) \le r_{i,t}^{dw} \qquad \forall i, \forall t, \forall s \quad (29)$$

$$0 \le \Delta P_{w,t}^w(s) \le P_{w,t}^{w,0}(s) \qquad \forall w, \forall t, \forall s \quad (30)$$

$$0 \le \Delta P_{d,t}^d(s) \le P_{d,t}^d \qquad \forall d, \forall t, \forall s \quad (31)$$

$$\mathbf{SF} \cdot \begin{bmatrix} \mathbf{KW} \cdot \left(\boldsymbol{P}_t^{w,0}(s) - \Delta \boldsymbol{P}_t^w(s) \right) + \\ \mathbf{KP} \cdot \boldsymbol{P}_t^G(s) - \mathbf{KD} \cdot \left(\boldsymbol{P}_t^d - \Delta \boldsymbol{P}_t^d(s) \right) \end{bmatrix} = \boldsymbol{F}^t(s) \qquad \forall t, \forall s \quad (32)$$

$$-\mu \overline{\boldsymbol{f}} \le \boldsymbol{F}^t(s) \le \mu \overline{\boldsymbol{f}} \qquad \forall t, \forall s \quad (33)$$

After the actual wind power output is observed and the unit dispatch decisions from the first stage are determined, the second-stage determines the corrective dispatch actions, including the redispatch of upward and downward reserves and the adjustment of wind power output. The objective in (24) is to minimize the expected penalty cost associated with these actions under the worst-case probability distribution. It is worth emphasising that the second-stage corrective decisions across all wind power scenarios aim to ensure that the first-stage unit dispatch decisions remain robust enough to maintain acceptable levels of wind power curtailment and load shedding. Based on

the unit commitment from the first stage, constraint (25) calculates the actual unit generation in wind power output scenario s, and constraint (26) ensures the power balance in wind power output scenario s. Based on the on and off status of each unit from the first-stage, constraint (27) limits the unit generation capacity in wind power output scenario s. Constraints (28) and (29) limit the deployment capacity of upward and downward reserves in wind power output scenario s. Constraints (30) and (31) limit wind power curtailment and load shedding levels in wind power output scenario s, respectively. Constraint (32) calculates the power flow in each line, which involves wind power curtailment and load shedding in wind power output scenario s. Constraint (33) limits the power flow in wind power output scenario s, which ensures that the line overloading ratio is within the limit.

To sum up, the TDRC model can be formulated as a tractable optimisation problem with objective function (34), subject to constraints (7)-(23) from the first-stage unit dispatch and constraints (25)-(33) from the second-stage corrective dispatch.

$$\begin{aligned}&\min \sum_{t=1}^{\mathrm{NT}}\sum_{i=1}^{\mathrm{NG}}\left(C_i^g P_{i,t}^g + S_i^{up} y_{i,t} + S_i^{dw} z_{i,t} + C_i^{up} r_{i,t}^{up} + C_i^{dw} r_{i,t}^{dw}\right) + \\ &\max_{p_s \in \mathcal{D}} \sum_{s=1}^{K} p_s . \min\left(\sum_{t=1}^{\mathrm{NT}}\sum_{d=1}^{\mathrm{ND}} C_d \Delta P_{d,t}^d(s) + \sum_{t=1}^{\mathrm{NT}}\sum_{w=1}^{\mathrm{NW}} C_w \Delta P_{w,t}^w(s)\right)\end{aligned} \tag{34}$$

The transformation of chance constraints (21)-(22) and the solution of the tractable problem will be discussed in the next section. Finally, a HPS algorithm is developed to solve the TDRC model and determine the optimal dispatch decisions for the system operator. In this paper, although wind power is used as a representative example of renewable energy uncertainty, the TDRC model can potentially be extended to other renewable sources, such as photovoltaic power from solar farms.

III. Hybrid Parallel Solution Methodology

A. Linearisation of Chance Constraints

In this paper, the wind power output is assumed to follow a Gaussian distribution, which is theoretically justified by the central limit theorem and empirically through short-term wind power output analyses [32-34]. Although the chance constraints (21)-(22) cannot be directly solved due to their nonlinear formulations, they can be further transformed into deterministic linear forms under the Gaussian distribution assumption. The transformation equations for these chance constraints are as follows:

Chance Constraint for Load Shedding: If the maximum available power output from units, wind power, and upward reserve capacity is insufficient to meet the load demand, load shedding will be required to ensure power balance in power systems. It is worth noting that constraint (21) can be equivalently transformed into equation (35).

$$\sum_{d=1}^{\mathrm{ND}} P_{d,t}^d \le \sum_{i=1}^{\mathrm{NG}} P_{i,t}^g + \sum_{i=1}^{\mathrm{NG}} r_{i,t}^{up} + \sum_{w=1}^{\mathrm{NW}} \overline{P}_{w,t}^w - \mathcal{Z}_{\mathrm{LSL}} \left(\sum_{w=1}^{\mathrm{NW}} {\sigma_{w,t}^w}^2\right)^{\frac{1}{2}} \quad \forall t \tag{35}$$

Hence, Eq. (35) is the deterministic equivalent of the chance constraint on load shedding. It is derived by applying quantile-based reformulation to convert the probabilistic constraint in (21) into a tractable deterministic formulation. In this equation, $\mathcal{Z}_{\mathrm{LSL}}$ denotes the standard normal quantile corresponding to the violation probability γ_{LSL}, and $\sigma_{w,t}^w$ represents the standard deviation of the wind power uncertainty for wind farm w at time t. This formulation ensures that the total available generation and upward reserve are sufficient to satisfy the load demand in at least $1-\gamma_{\mathrm{LSL}}$ of all scenarios, thereby guaranteeing system reliability under uncertain wind power output conditions.

Chance Constraint for Wind Power Curtailment: If the excess power output from units, wind power, and downward reserve cannot be absorbed by the load demand, wind power will be curtailed in power systems. However, to guarantee the wind power utilisation, the wind power utilisation rate is required not to fall below its minimum utilisation rate β_w. Note that this chance constraint (22) can be further reformulated into the following deterministic form:

$$\sum_{i=1}^{\mathrm{NG}} P_{i,t}^g - \mathcal{Z}_{\mathrm{WPCL}} \left(\sum_{w=1}^{\mathrm{NW}} (\beta_w \sigma_{w,t}^w)^2\right)^{\frac{1}{2}} \le -\beta_w \sum_{w=1}^{\mathrm{NW}} \overline{P}_{w,t}^w + \sum_{i=1}^{\mathrm{NG}} r_{i,t}^{dw} + \sum_{d=1}^{\mathrm{ND}} P_{d,t}^d \quad \forall t \tag{36}$$

Here, Eq. (36) represents the deterministic equivalent of the chance constraint on wind power curtailment. It is derived through the quantile-based reformulation of the probabilistic constraint in (22), converting the stochastic inequality into a tractable deterministic formulation. In this equation, $\mathcal{Z}_{\mathrm{WPCL}}$ denotes the standard normal quantile associated with the violation probability γ_{WPCL}, and $\sigma_{w,t}^w$ denotes the standard deviation of wind power uncertainty for wind farm w at time t. The parameter β_w denotes the minimum acceptable wind power utilisation rate. This formulation ensures that, in at least $1-\gamma_{\mathrm{WPCL}}$ of all scenarios, the downward reserve and load demand are sufficient to absorb wind power fluctuations, thereby keeping the wind power curtailment within its allowable level.

B. Linearisation of L_1 and L_∞ norms

Similarly, L_1 and L_∞ norms are transformed into linear formulations to facilitate the optimisation solution.

For the L_1 norm case, the nonlinear term $\sum_{s=1}^{K}\left|p_s - p_s^0\right| \le \theta$ in $\mathcal{D}$ is equivalent to constraints (37)-(38).

$$\sum_{s=1}^{K} h_s \le \theta_1 \tag{37}$$

$$\begin{cases} h_s \ge p_s - p_s^0 \\ h_s \ge p_s^0 - p_s \end{cases} \quad \forall s \tag{38}$$

For the L_∞ norm case, the nonlinear term $\max_{1\le s\le K}\left|p_s - p_s^0\right| \le \theta$ in $\mathcal{D}$ can be replaced by the following constraint (39).

$$\begin{cases} p_s - p_s^0 \le \theta_\infty \\ p_s^0 - p_s \le \theta_\infty \end{cases} \quad \forall s \tag{39}$$

C. *Overall framework of the HPS Algorithm*

For simplicity and without loss of generality, the TDRC model can be represented in the following compact form:

$$\min_{\boldsymbol{x},\boldsymbol{y}} \left\{ \boldsymbol{a}^{\mathrm{T}}\boldsymbol{x} + \boldsymbol{b}^{\mathrm{T}}\boldsymbol{y} + \max_{p_s \in \mathcal{D}} \sum_{s=1}^{K} \hat{p}_s^n \min_{\mathbf{z}_s \in \boldsymbol{Y}(\boldsymbol{x},\boldsymbol{y},\boldsymbol{\xi}_s)} \boldsymbol{h}^{\mathrm{T}}\mathbf{z}_s^n \right\} \tag{40}$$

subject to:

$$\boldsymbol{A}\boldsymbol{x} \le \boldsymbol{e} \qquad \boldsymbol{x} \in \{\mathbf{0},\mathbf{1}\} \tag{41}$$

$$\boldsymbol{B}\boldsymbol{x} + \boldsymbol{C}\boldsymbol{y} \le \boldsymbol{d} \tag{42}$$

$$\boldsymbol{F}\boldsymbol{x} + \boldsymbol{D}\boldsymbol{y} + \boldsymbol{G}\boldsymbol{\xi}_s + \boldsymbol{H}\mathbf{z}_s \le \boldsymbol{g} \qquad \forall s \tag{43}$$

where vector $\boldsymbol{x}$ represents binary variables and vector $\boldsymbol{y}$ represents continuous variables in the first-stage problem. Vector $\mathbf{z}_s$ represents continuous variables in the second-stage problem. Notably, vector $\boldsymbol{\xi}_s$ represents the wind power output scenario, i.e., $P_{i,t}^{w,0}(s)$. Matrix $\boldsymbol{A}$ and vector $\boldsymbol{e}$ represent the coefficient matrices and constant vectors of constraints (7)-(10), respectively. Matrices $\boldsymbol{B}$, $\boldsymbol{C}$, and vector $\boldsymbol{d}$ denote the coefficient matrices and constant vectors of constraints (11)-(22), respectively. Matrices $\boldsymbol{F}$, $\boldsymbol{D}$, $\boldsymbol{G}$, $\boldsymbol{H}$, and vector $\boldsymbol{g}$ are the coefficient matrices and constant vectors of constraints (25)-(33), respectively.

The developed HPS algorithm is a hybrid parallel-based approach that does not rely on duality information, and it incorporates the advantages of the BD and C&CG methods to improve computational efficiency. To solve the overall problem, the TDRC model is first decomposed into a master problem **P0** and a sub-problem **P1**, as described in detail below.

Master problem **P0:**

$$\min_{\boldsymbol{x},\boldsymbol{y},\mathbf{z}_s^n,\eta} \boldsymbol{a}^{\mathrm{T}}\boldsymbol{x} + \boldsymbol{b}^{\mathrm{T}}\boldsymbol{y} + \eta \tag{44}$$

subject to:

$$\boldsymbol{A}\boldsymbol{x} \le \boldsymbol{e} \tag{45}$$

$$\boldsymbol{B}\boldsymbol{x} + \boldsymbol{C}\boldsymbol{y} \le \boldsymbol{d} \tag{46}$$

$$\eta \ge \max_{p_s \in \mathcal{D}} \sum_{s=1}^{K} \hat{p}_s^n \min_{\mathbf{z}_s^n \in \boldsymbol{Y}(\boldsymbol{x},\boldsymbol{y},\boldsymbol{\xi}_s)} \boldsymbol{h}^{\mathrm{T}}\mathbf{z}_s^n \qquad \forall n \le r, \forall s \tag{47}$$

$$\boldsymbol{F}\boldsymbol{x} + \boldsymbol{D}\boldsymbol{y} + \boldsymbol{G}\boldsymbol{\xi}_s + \boldsymbol{H}\mathbf{z}_s^n \le \boldsymbol{g} \qquad \forall n \le r, \forall s \tag{48}$$

$$\eta \ge \sum_{s=1}^{K} \hat{p}_s^n \left(\boldsymbol{h}^{\mathrm{T}}\mathbf{z}_s^n + \boldsymbol{v}^{\mathrm{T}}\boldsymbol{t}_s^n \right) + \sum_{s=1}^{K} \hat{p}_s^n \hat{\boldsymbol{\pi}}_{n,s}^{\mathrm{T}} \left(\boldsymbol{y} - \hat{\boldsymbol{y}}_n' \right) \qquad \forall n \le r, \forall s \tag{49}$$

where $\boldsymbol{\pi}_{n,s}$ denotes the dual variable associated with the following sub-problems. n represents the current iteration number. Constraints (47)-(48) represent the C&CG cut, and constraint (49) represents the Benders cut.

The minimisation and summation operations corresponding to the expected term can be interchanged due to the independence of different scenarios $\boldsymbol{\xi}_s$. Hence, the second-stage problem can be further decomposed into several smaller-scale sub-problems without requiring the dual problem information, which can be solved in parallel for computational efficiency.

Sub-problem **P1**:

$$f_{\mathrm{sp}}(\hat{\boldsymbol{x}}_n, \hat{\boldsymbol{y}}_n) = \max_{p_s \in \mathcal{D}} \sum_{s=1}^{K} \hat{p}_s^n \min_{z_s^n \in \boldsymbol{Y}(\boldsymbol{x},\boldsymbol{y},\boldsymbol{\xi}_s)} \boldsymbol{h}^{\mathrm{T}}\mathbf{z}_s^n + \boldsymbol{v}^{\mathrm{T}}\boldsymbol{t}_s^n \tag{50}$$

subject to:

$$\boldsymbol{F}\hat{\boldsymbol{x}}_n + \boldsymbol{D}\boldsymbol{y}_n' + \boldsymbol{G}\boldsymbol{\xi}_s + \boldsymbol{H}\mathbf{z}_s^n \le \boldsymbol{g} \qquad \forall n \le r, \forall s \tag{51}$$

$$\boldsymbol{y}' = \hat{\boldsymbol{y}}_n + \boldsymbol{t}_{n,s}^{+} - \boldsymbol{t}_{n,s}^{-} \qquad \boldsymbol{\pi}_{n,s} \qquad \forall n \le r, \forall s \tag{52}$$

$$\boldsymbol{t}_{n,s}^{+}, \boldsymbol{t}_{n,s}^{-} \ge 0 \qquad \forall n \le r, \forall s \tag{53}$$

where $\boldsymbol{t}_{n,s}^{+}$ and $\boldsymbol{t}_{n,s}^{-}$ are auxiliary positive variables, which are introduced only in the BD algorithm. Eq. (52) relaxes the coupling variables between the first-stage and second-stage problems to guarantee the feasibility of sub-problems in the BD algorithm. In addition, $\boldsymbol{t}_s^n$ denotes $\boldsymbol{t}_{n,s}^{+} + \boldsymbol{t}_{n,s}^{-}$. $\boldsymbol{v}$ is a large positive vector. $\boldsymbol{\pi}_{n,s}$ is the dual variable vector. When the sub-problems are solved under the C&CG algorithm, the auxiliary variables $\boldsymbol{t}_{n,s}^{+}$ and $\boldsymbol{t}_{n,s}^{-}$ are both set to $\mathbf{0}$. Finally, a master problem and sub-problems are iteratively solved until the convergence threshold is met. It should be emphasised that the reformulated problems are convex mixed-integer programs with linearised chance constraints and ambiguity set representations. The HPS algorithm iteratively solves a decomposed master problem and multiple sub-problems, where each sub-problem is convex and feasible under the worst-case probability distribution.

Based on the convergence properties of the BD and C&CG methods [35, 36], the HPS algorithm can guarantee finite-step convergence to the global optimum. The overall steps of solution algorithm are outlined as follows.

Algorithm 1: *Hybrid Parallel Solution (HPS) Algorithm*

1. **Initialise**: Set the optimality tolerance gap $\varepsilon \leftarrow 0.0001$. Initialise: $L_{\mathrm{B}} \leftarrow -\infty$, $U_{\mathrm{B}} \leftarrow +\infty$, and $n \leftarrow 0$. Also, the initial solution of sub-problem **P1** is set to $(\hat{p}_s^n, \hat{\mathbf{z}}_s^n, \hat{\boldsymbol{\pi}}_{n,s}^{\mathrm{T}})$.
2. **If** $\left|U_{\mathrm{B}} - L_{\mathrm{B}}\right| / U_{\mathrm{B}} > \varepsilon$: **do**
3. Solve master problem **P0** based on $(\hat{p}_s^n, \hat{\mathbf{z}}_s^n, \hat{\boldsymbol{\pi}}_{n,s}^{\mathrm{T}})$ and obtain the optimal solution $(\hat{\boldsymbol{x}}_{n+1}, \hat{\boldsymbol{y}}_{n+1}, \hat{\eta}_{n+1})$;
4. Update $L_{\mathrm{B}} \leftarrow \boldsymbol{a}^{\mathrm{T}}\hat{\boldsymbol{x}}_{n+1} + \boldsymbol{b}^{\mathrm{T}}\hat{\boldsymbol{y}}_{n+1} + \hat{\eta}_{n+1}$;
5. Substitute $(\hat{\boldsymbol{x}}_{n+1}, \hat{\boldsymbol{y}}_{n+1})$ into sub-problem **P1** and then solve **P1** to obtain the optimal solution $(\hat{p}_s^{n+1}, \hat{\mathbf{z}}_s^{n+1}, \hat{\boldsymbol{\pi}}_{n+1,s}^{\mathrm{T}})$;
6. Update the worst-case probability $\hat{p}_s^{n+1}$;
7. Update $U_{\mathrm{B}} \leftarrow \min\{U_{\mathrm{B}}, \boldsymbol{a}^{\mathrm{T}}\hat{\boldsymbol{x}}_{n+1} + \boldsymbol{b}^{\mathrm{T}}\hat{\boldsymbol{y}}_{n+1} + f_{\mathrm{sp}}(\hat{\boldsymbol{x}}_{n+1}, \hat{\boldsymbol{y}}_{n+1})\}$;
8. Create variables $\mathbf{z}_s^{n+1}$ and add constraints

$$\eta \ge \max_{p_s \in \mathcal{D}} \sum_{s=1}^{K} \hat{p}_s^n \min_{\mathbf{z}_s^{n+1} \in \boldsymbol{Y}(\boldsymbol{x},\boldsymbol{y},\boldsymbol{\xi}_s)} \boldsymbol{h}^{\mathrm{T}}\mathbf{z}_s^{n+1}$$

$$\boldsymbol{F}\boldsymbol{x} + \boldsymbol{D}\boldsymbol{y} + \boldsymbol{G}\boldsymbol{\xi}_s + \boldsymbol{H}\mathbf{z}_s^{n+1} \le \boldsymbol{g}$$

$$\eta \ge \sum_{s=1}^{K} \hat{p}_s^{n+1} \left(\boldsymbol{h}^{\mathrm{T}}\mathbf{z}_s^{n+1} + \boldsymbol{v}^{\mathrm{T}}\boldsymbol{t}_s^{n+1} \right) + \sum_{s=1}^{K} \hat{p}_s^{n+1} \hat{\boldsymbol{\pi}}_{n+1,s}^{\mathrm{T}} \left(\boldsymbol{y} - \hat{\boldsymbol{y}}_{n+1}' \right)$$

to master problem;

9. $n \leftarrow n+1$
10. **Else**: **do**
11. Output the optimal dispatch solutions.
12. **End**

IV. Case Studies

This section conducts case studies to verify the superiority of the proposed approach over other methods. Meanwhile, a Monte Carlo algorithm is employed to generate independent wind power output scenarios that fit the historical data, and these scenarios are referred to as data samples. In addition, the probabilistic distance algorithm is used to group wind power output scenarios into K clusters. The TDRC model is solved using the Gurobi 10.0.3 solver in MATLAB 2019b.

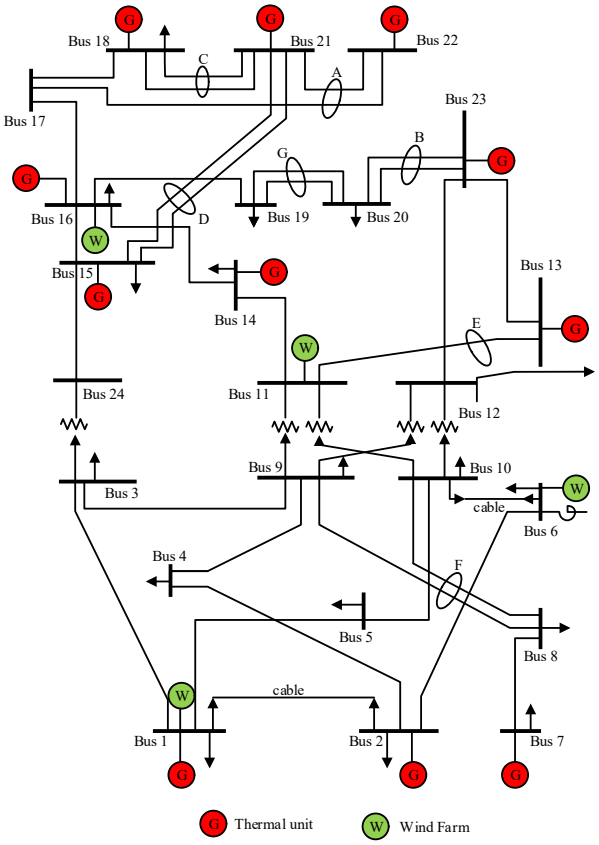

Fig. 3. Architecture diagram of the IEEE 24-bus system.

***(1) IEEE 24-bus System*:** This system has 17 loads, 10 units, and 38 lines, and its peak load level is 2,850 MW. In addition, there are 4 wind farms at buses 1, 6, 11, and 16, respectively, as shown in Fig. 3. This results in a wind power penetration level of over 28%. Furthermore, the wind power utilisation rate is set to 85%, i.e., $\beta_w = 0.85$.

A. Impact of the Data Sample Size

This case analyses the impact of data sample size on the TDRC model by varying the data sample size from 10 to 5000. Additionally, the load shedding and wind power curtailment levels are held constant at 0.050 and 0.100, respectively. The number of clusters is $K = 5$, and the confidence level α is 0.95. Table II shows the simulation results under different data sample sizes.

It is observed that the total cost decreases as the data sample size increases. For example, if the data sample size is equal to 1000 (i.e., $N_S = 1000$), the total cost is \$648,702.05, while it reduces to \$648,021.13 when $N_S = 3000$. This decrease occurs because a larger sample size shrinks the designed ambiguity confidence set, making the dispatch strategy less conservative. Moreover, in the proposed TDRC model, as the sample size increases, the total cost almost approaches that of the SP and Wasserstein-based DRO models. This is because, with more available data samples, the wind power output probability distribution becomes closer to the true distribution, while diminishing the difference in performance between the designed ambiguity confidence set and the Wasserstein-based ambiguity set. The results further indicate that the dispatch decisions obtained in the RO model incur the highest total cost, which results from its consideration of the worst-case scenario to make overly conservative dispatch decisions. Since the KL-divergence-based ambiguity set exponentially reweights tail scenarios, increasing the likelihood of extreme events, the KL-based DRO model tends to yield more conservative dispatch decisions with a higher total cost. However, the proposed TDRC approach can yield less conservative decisions, achieving greater cost effectiveness. Meanwhile, the results indicate that if the TDRC model is partially designed with an ambiguity confidence set using only the L_1 norm (denoted as the L_1-based DRO model), the total cost becomes higher with more conservative dispatch decisions than the full TDRC model (i.e., the proposed TDRC approach), which combines the L_1 norm and the L_∞ norm, under the same data sample size. This is due to the fact that their combination yields a smaller ambiguity confidence set compared to that derived by only L_1 norm. To sum up, the proposed TDRC approach is superior to other approaches in adjusting its conservativeness.

TABLE II.
Comparison of Total Cost Between Various Models Under Different Data Sample Sizes ($)

# of data	TDRC	L_1	SP [12]	RO [14]	KL [20]	Wasserstein [21]
10	651277.42	651507.18	649909.42	653496.95	651092.04	650031.56
50	650010.34	650312.81	649698.17	653496.95	650297.61	649766.32
200	648728.16	648777.30	648679.37	653496.95	648909.61	648702.77
1000	648702.05	648711.84	648688.07	653496.95	648810.91	648702.02
3000	648021.13	648025.28	648016.90	653496.95	648810.65	648025.93
5000	647552.45	647554.39	647550.81	653496.95	647590.03	647555.59

† The L_1-, KL- and Wasserstein-based methods correspond to different DRO models. The full names of these models are not provided in the table due to space limitations.

B. Impact of the Confidence Level

This case examines the impact of the confidence level (i.e., α) on the conservativeness of the TDRC model. Meanwhile, the confidence level α influences the scalar parameter θ in equations (4) and (5), which in turn affects the conservativeness of dispatch decisions in power systems. To analyse their effects, load shedding and wind power curtailment levels are set to 0.025 and 0.050, respectively. The size of data samples is assumed to be 1000, i.e., $N_S = 1000$, and the number of clusters K is 5. Table III shows the simulation results under different parameters α and θ.

From the simulation results on the left side of Table III, it is observed that as α increases, the total cost also increases. This occurs because a larger α causes the designed ambiguity confidence set to include more unknown probability distributions of wind power output. Thus, with a higher confidence level, the TDRC model makes more conservative decisions due to the consideration of additional unknown probability distributions, which increases the total cost. When the TDRC model considers only the L_1 norm to construct the ambiguity confidence set (i.e., L_1-based DRO model), the total cost in the L_1-based model is higher than that in the proposed TDRC model. Similarly, from the simulation results on the right side of Table III, it is observed that a confidence set based on a larger θ can contain more extreme probability distributions, thereby leading to a higher total cost. Furthermore, the total cost obtained in the L_∞-based DRO model is higher than that produced in the TDRC model. This is because the designed confidence set, which integrates both the L_1 norm and the L_∞ norm, is smaller than the ambiguity confidence set designed based on either L_1 norm or L_∞ norm alone, making the TDRC model less conservative. This indicates that the proposed approach is superior to other approaches in designing a suitable ambiguity confidence set with minimum total cost. In addition, the TDRC model offers an alternative way for the system operator to flexibly regulate the conservativeness of the TDRC model by directly adjusting the confidence level α.

TABLE III.
COMPARISON OF TOTAL COST BETWEEN DIFFERENT CONDITIONS UNDER DIFFERENT PARAMETERS ($)

α	TDRC	L_1	θ	TDRC	L_∞
0.1	657024.06	657027.49	0.1	657164.91	657459.90
0.2	657024.32	657027.92	0.2	657310.40	657880.66
0.3	657024.62	657028.41	0.3	657457.44	657995.55
0.4	657024.96	657028.96	0.4	657602.27	658010.81
0.5	657025.37	657029.63	0.5	657685.31	658015.51
0.6	657025.87	657030.45	0.6	657761.87	658016.70
0.7	657026.51	657031.50	0.7	657841.06	658017.90
0.8	657027.41	657032.98	0.8	657901.86	658022.70
0.9	657028.96	657035.51	0.9	657959.68	658018.22
0.99	657034.09	657043.92	0.99	657994.60	658018.22

† The L_1- and L_∞-based methods correspond to different DRO models. The full names of these models are not provided in the table due to space limitations.

C. Impact of the Wind Power Output Scenario Cluster

The number of clusters K for wind power output scenarios may have direct impacts on the dispatch decisions, which is reflected in the total cost. Thus, the number of clusters K is varied from 5 to 15 with an incremental step of 2. The confidence level α is set to 0.99. In addition, the data sample size is 1000, i.e., $N_S = 1000$, and wind power curtailment and load shedding levels both remain constant at 0.05.

TABLE IV.
COMPARISON OF TOTAL COST UNDER DIFFERENT WIND POWER OUTPUT SCENARIO CLUSTERS K ($)

K	TDRC	L_1	SP [12]	RO [14]	KL [20]	Wasserstein [21]
5	648918.03	648928.99	648901.63	655060.27	649031.23	648916.90
7	648908.48	648927.61	648887.54	655060.27	649028.68	648902.77
9	648877.32	648905.17	648852.03	655060.27	648993.53	648867.22
11	648830.26	648866.45	648799.56	655060.27	648946.01	648814.85
13	648823.08	648867.20	648786.58	655060.27	648944.94	648801.83
15	648755.48	648869.36	648697.92	655060.27	648950.55	648728.25

† The L_1-, KL- and Wasserstein-based methods correspond to different DRO models. The full names of these models are not provided in the table due to space limitations.

It is clear from Table IV that a larger cluster number K for wind power output scenarios can result in a decrease in the total cost. For example, the total cost is \$648,908.48 when K is set to 7, whereas the total cost decreases to \$648,877.32 if it is increased to 9. This is due to the fact that a larger number of clusters K can capture more typical scenarios to support the proposed TDRC model in determining more accurate dispatch decisions, which become more effective as an increasing number of typical wind power output scenarios are captured. These typical scenarios can support the TDRC model in making cost-effective decisions, and the proposed approach also offers an opportunity for the system operator to adjust the conservativeness of TDRC model by varying the number of clusters K. Although the Wasserstein-based DRO model yields a slightly lower total cost than the TDRC model as the number of scenario clusters increases, the results remain very close. Nevertheless, the Wasserstein approach entails a higher computational complexity due to transport variables and nonlinear coupling, whereas the proposed approach achieves comparable costs with lower complexity. Meanwhile, it is interesting to note that the total cost in the SP model is lower than that in the TDRC model. This is because the proposed TDRC model accounts for the worst-case probability distribution, thereby leading to more conservative dispatch decisions. Nevertheless, it still outperforms both the L_1-based DRO, KL-based DRO and the RO models in terms of total cost, highlighting its superiority in adapting to uncertainty under different wind power output scenario clusters.

D. Impact of the Load Shedding Level

The impact of load shedding levels on the total cost and the upward and downward reserve costs is examined by varying the

load shedding level from 0.005 to 0.200, i.e., $\gamma_{\mathrm{LSL}} \in [0.005, 0.200]$. The wind power curtailment level remains constant at 0.025. The size of data samples is 1000, i.e., $N_{\mathrm{S}} = 1000$. A confidence level of $\alpha = 0.99$ is used and the data is divided into five clusters, i.e., $K = 5$.

Table V presents the total cost and the upward and downward reserve cost at different load shedding levels. The total cost decreases as the load shedding level increases. For instance, the total cost is \$667,465.93 at a load shedding level of 0.01, whereas it decreases to \$660,238.20 at a load shedding level of 0.020. In addition, it is observed that the load shedding level can have a more significant impact on the upward reserve than on the downward reserve. This is due to the fact that when the available power is insufficient to meet the load demand, it necessitates providing more upward reserve from units to mitigate load shedding, resulting in a higher upward reserve cost compared to the downward reserve cost. Thus, the upward reserve cost is consistently higher than the downward reserve cost at all load shedding levels. Additionally, Fig. 4 shows the ratio of upward and downward reserve costs to the total cost, respectively. The ratio of upward reserve cost to total cost gradually decreases as the load shedding level increases, since a larger load shedding level can relieve the requirement for the upward reserve provided by units. However, the ratio of downward reserve cost to total cost remains around 0.2% when the load shedding level is greater than or equal to 0.100, since the requirement for downward reserve remains almost unchanged. This suggests that the proposed approach provides an effective method for selecting a load shedding level based on various cost budgets.

TABLE V.
EFFECTS OF THE LOAD SHEDDING LEVELS (\$)

γ_{LSL}	Total cost	Upward reserve cost	Downward reserve cost
0.005	674149.29	13978.41	5638.37
0.010	667465.93	12946.95	4678.07
0.020	660238.20	12276.32	3490.63
0.025	657766.96	12024.44	3102.74
0.050	649642.65	10920.20	2063.06
0.100	640864.88	9331.53	1244.63
0.200	632168.01	6666.57	1239.18

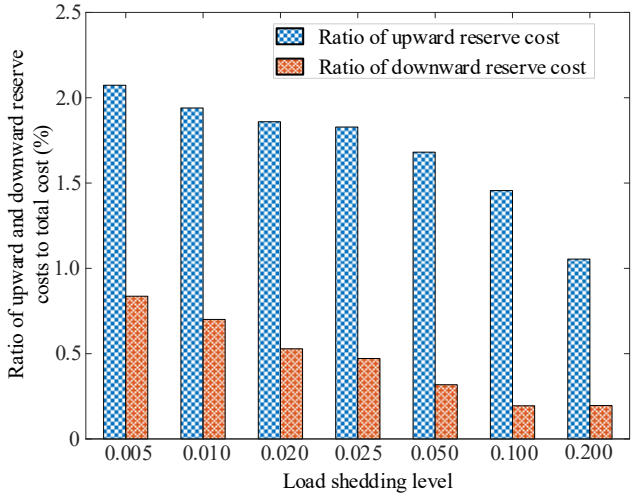

Fig. 4. Ratio of upward and downward costs to total cost under different load shedding levels.

E. *Impact of the Wind Power Curtailment Level*

This case further investigates the impact of wind power curtailment levels on total and upward and downward reserve costs. Therefore, the wind power curtailment level is varied from 0.005 to 0.200, i.e., $\gamma_{\mathrm{WPCL}} \in [0.005, 0.200]$. The confidence level α is maintained at 0.99, and the size of data samples is 1000, i.e., $N_{\mathrm{S}} = 1000$. The load shedding level is fixed at 0.025, and the number of clusters K is set to 5.

TABLE VI.
EFFECTS OF THE WIND POWER CURTAILMENT LEVEL (\$)

γ_{WPCL}	Total cost	Upward reserve cost	Downward reserve cost
0.005	660023.01	12190.88	6696.47
0.010	658985.04	12024.44	5279.21
0.020	658043.22	12024.44	3660.20
0.025	657766.96	12024.44	3102.74
0.050	657034.09	11981.49	1532.13
0.100	656720.83	11841.55	604.25
0.200	656640.27	11752.61	230.93

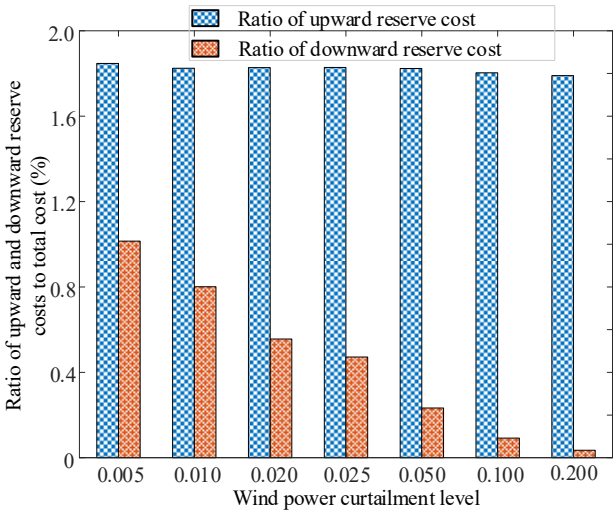

Fig. 5. Ratio of upward and downward reserve costs to total cost under different wind power curtailment levels.

From Table VI, the results show that the downward reserve cost decreases as the level of wind power curtailment increases. It is observed that the total cost is \$149,194.36 when the wind power curtailment level is 0.010, whereas the total cost is \$103,439.95 when the curtailment level is 0.020. It is worth noting that the wind power curtailment level does not significantly affect the upward reserve cost. The primary cause is that the downward reserve is mainly used for regulating wind power output. In particular, in high wind situations where the total generation exceeds the system load, both downward reserve and wind power curtailment actions are taken to ensure power balance. The higher the wind power curtailment level, the less downward reserve is required for the downward regulation of excessive generation. This indicates that the relationship between wind power curtailment and downward reserve is stronger than that with the upward reserve. Similarly, Fig. 5 also shows the ratio between upward and downward reserve costs and total cost. With a higher wind power curtailment level, the ratio between downward reserve cost and total cost becomes lower. In contrast, the ratio between upward reserve cost and total cost is maintained at around 1.82%, since

the requirement for upward reserve shows little variation. Similarly, the wind power curtailment level can be reasonably selected to adjust the TDRC model's upward and downward reserve cost and dispatch decisions according to different operational cost budgets of power systems.

***(2) IEEE 118-bus System*:** To verify the benefits of the proposed TDRC approach in large-scale power systems, additional numerical simulations are performed on the IEEE 118-bus system with a peak load demand of 6,600 MW. Fig. 6 illustrates the locations of five wind farms with an installed capacity of 200 MW, which are at buses 1, 29, 60, 92 and 118.

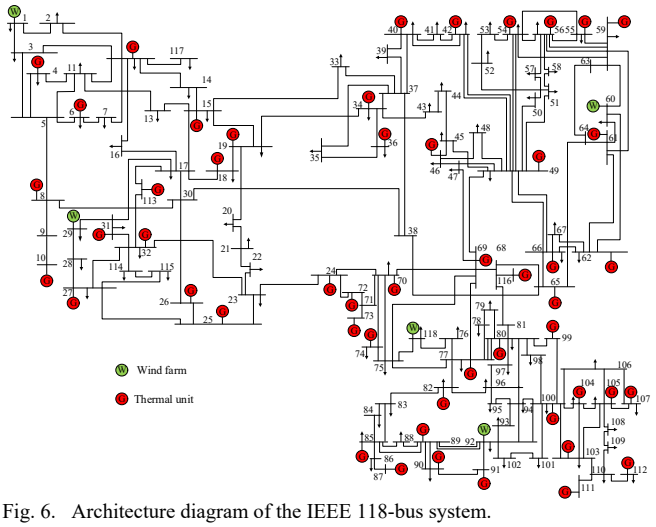

Fig. 6. Architecture diagram of the IEEE 118-bus system.

F. Impact of the Wind Power Utilisation Rate

This case study examines the impact of wind power utilisation rate β_w on the TDRC model. From chance constraint (22), it is observed that β_w can affect the system operator's dispatch decisions. Accordingly, the wind power utilisation rate β_w is varies from 0.80 to 0.95. Similarly, the size of data samples is 1000, i.e., $N_S = 1000$. The confidence level α is assumed to be 0.99, and the number of clusters K is 5. The wind power curtailment level is set within the interval [0.005, 0.200], while the load shedding level is fixed at 0.025.

Table VII shows the total cost under different wind power utilisation rates. For a given wind power curtailment level, the total cost decreases as the wind power utilisation rate increases. This is because, to guarantee a higher wind power utilisation rate, the system operator needs to dispatch more unit generation and store more reserve to absorb wind power. In contrast to the downward reserve cost, the upward reserve cost may decrease as the wind power utilisation rate increases. When γ_{WPCL} is fixed at 0.050, the upward reserve cost is \$21,844.73 if β_w is set to 0.85, while it is \$24,798.37 when β_w is 0.95. However, the overall trend of the upward reserve cost still shows an increase with the increase in the wind power utilisation rate. Moreover, the wind power curtailment level has less effect on the upward reserve cost compared to the downward reserve cost. This is because the upward reserve is more sensitive to the load shedding level than to the wind power curtailment level, as clarified above. Meanwhile, Fig. 7 shows the corresponding total cost of the proposed TDRC model under different combinations when β_w is 0.95. This means that the system operator can flexibly determine dispatch decisions based on the cost budget by considering different combination scenarios.

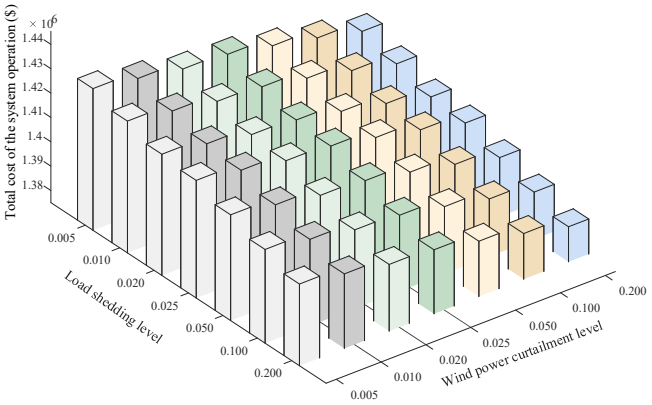

Fig. 7. Total cost for the power system operation under different combination conditions.

TABLE VII.
COMPARISON OF TOTAL COST UNDER DIFFERENT WIND POWER UTILISATION RATES ($)

$\gamma_{\text{LSL}} = 0.025$	$\beta_w = 0.80$			$\beta_w = 0.85$			$\beta_w = 0.95$		
γ_{WPCL}	Total cost	Upward reserve cost	Downward reserve cost	Total cost	Upward reserve cost	Downward reserve cost	Total cost	Upward reserve cost	Downward reserve cost
0.005	1401423.89	23067.36	41.62	1407116.40	24888.59	6797.27	1423293.58	24827.53	23992.61
0.010	1400915.19	20845.10	0	1404937.16	24798.49	4119.58	1420351.45	24798.37	20999.89
0.020	1400553.56	18812.05	0	1402646.16	24798.50	1183.80	1417129.41	24798.37	17718.73
0.025	1400490.52	18226.90	0	1401978.73	24748.48	224.82	1416032.86	24827.53	16588.95
0.050	1400350.75	17026.52	0	1401116.18	21844.73	0	1412428.20	24798.37	12802.98
0.100	1400255.66	16175.74	0	1400542.07	18771.07	0	1408487.07	24817.20	8440.11
0.200	1400182.96	15561.17	0	1400329.04	16852.15	0	1404176.85	24798.49	3187.84

G. Comparative Analysis

In this case, the TDRC model is further compared with other models to validate the performance of the proposed approach. The size of data samples is set to range from 10 to 5000. The confidence level α is 0.95. Wind power curtailment and load shedding levels are held constant at 0.05 and 0.025, respectively. Table VIII shows the simulation results under different data sample sizes.

It can be observed that as the size of data samples increases, the total cost decreases. For the same data sample size, the total

cost in the TDRC model is lower than that of the L_1-based, KL-based DRO and RO models, except for that in the Wasserstein-based DRO and SP models. However, with an increase in available data samples, the proposed TDRC model almost converges to the Wasserstein-based DRO and SP models, as an increased number of available data samples results in a more accurate probability distribution estimation, while reducing the performance gap between the combined L_1 and L_∞ norms ambiguity confidence set and the Wasserstein-based ambiguity set. Thus, the proposed TDRC approach has advantages in determining dispatch decisions for the system operator in the unit commitment problem when compared with other methods.

Meanwhile, it is worth mentioning that the maximum solution time is 240.68 seconds for the case presented in Table VIII, which is significantly lower than the 259.64 seconds required by the C&CG algorithm. This is also well within the day-ahead dispatch time scale of 24 hours. This is due to the fact that the proposed HPS algorithm combines the advantages of BD and C&CG approaches, thus resulting in shorter computational time. This indicates that the proposed HPS algorithm enhances computational efficiency in solving large-scale problems. Furthermore, this case validates the scalability and superiority of the proposed TDRC approach for large-scale power systems.

TABLE VIII.
SIMULATION RESULTS BETWEEN DIFFERENT APPROACHES IN IEEE 118-BUS SYSTEM ($)

# of data	TDRC	L_1	SP [12]	RO [14]	KL [20]	Wasserstein[21]
10	1403286.45	1403540.81	1402095.34	1415128.72	1403353.64	1402179.72
50	1400655.17	1400849.53	1400305.40	1415128.72	1401236.70	1400358.33
200	1400676.48	1400773.77	1400574.60	1415128.72	1400992.37	1400612.39
1000	1400179.18	1400200.20	1400154.81	1415128.72	1400343.59	1400177.81
3000	1399690.23	1399783.22	1399758.13	1415128.72	1399747.70	1399692.40
5000	1399640.59	1399654.70	1399638.69	1415128.72	1399676.05	1399642.52

† The L_1-, KL- and Wasserstein-based methods correspond to different DRO models. The full names of these models are not provided in the table due to space limitations.

***(3) Cyber-Physical Power System Dispatch Platform*:** To further verify the practical applicability of the proposed TDRC approach, additional experiments are performed on a practical 126-bus system using a CPPS dispatch platform. This system has 91 loads, 54 units, and 194 lines, and its peak load level is 3,668 MW. In addition, there are 18 wind farms at buses 4, 6, 10, 12, 15, 18, 19, 24, 25, 26, 31, 32, 46, 69, 99, 116, 119 and 120, respectively. Detailed information about this 126-bus system can be found in [37]. Meanwhile, the architectural diagram of the CPPS dispatch platform is shown in Fig. 8, and this platform is mainly composed of three parts: the physical layer, the cyber layer and the control centre.

*1) **Physical layer***: In the developed CPPS dispatch platform, this physical layer comprises the digital power system and remote terminal unit (RTU). This digital power system simulates the operation state of the system and serves as the data source in the physical layer. It requires accurate modelling of the dynamic behaviour of power systems. Here, we simulate a practical 126-bus power system. The RTU serves as the interface between the physical and cyber layers. It not only acquires measurements from the digital power system and transmits them to the control centre through the cyber layer but also receives control commands from the control centre and executes them at the physical layer.

*2) **Cyber layer***: This cyber layer comprises the network switch and the front-end processor (FEP). The network switch serves as the communication hub, forwarding data packets from the RTU to the FEP and ensuring reliable data transmission within the system. Note that the measurements collected by the RTU are transmitted to the cyber layer through the IEC 60870-5-104 protocol. The FEP receives the data from multiple RTUs, decodes and parses the communication frames, and converts them into a unified data format which is then published to control systems such as SCADA via the MQTT protocol, allowing the control centre to subscribe to and utilise the data efficiently.

*3) **Control centre***: In this platform, the control centre is composed of the SCADA system and the EMS. These two systems are interconnected through the network switch, and in the CPPS dispatch platform, their communication is implemented via the HTTPS protocol, which ensures secure and reliable data exchange. The SCADA system performs real-time monitoring, visualisation, and basic control of the power systems with wind power and units, while the EMS conducts higher-level analysis such as power flow calculation, wind power forecasting, and optimal dispatch based on the operational data provided by SCADA system.

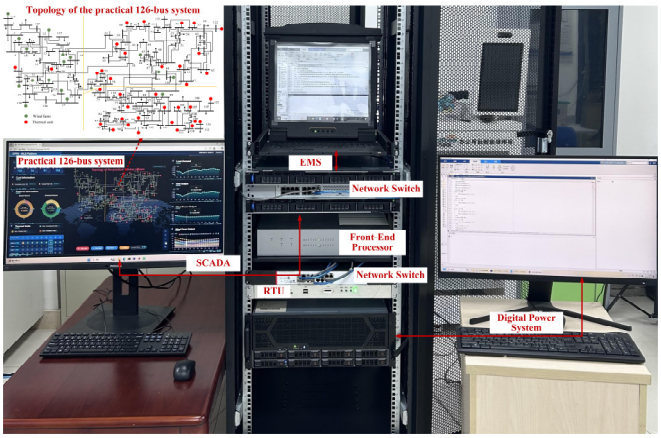

Fig. 8. Architecture of CPPS dispatch platform based on the practical 126-bus system.

Based on the CPPS dispatch platform, a practical 126-bus power system can be simulated within a realistic dispatch environment that integrates the SCADA system and EMS. In this test, the 24-hour load fluctuation curve is shown in Fig. 8. Meanwhile, based on 5-minute historical wind power output

measurements, a gradient boosting regression (GBR) model is employed with lag and rolling statistical features to forecast the 24-hour wind power output. This forecasting process is not the focus of this paper and does not affect the essence of our proposed approach. Note that the load shedding and wind power curtailment levels are set to 0.005. In addition, the confidence level α is 0.99, and the wind power utilisation rate is set to 95%, i.e., $\beta_w = 0.95$. The number of clusters is $K = 7$, and the size of data samples is 1000, i.e., $N_S = 1000$. The test results under different models are shown in Table IX.

TABLE IX.
SIMULATION RESULTS UNDER DIFFERENT MODELS IN A PRACTICAL 126-BUS SYSTEM

Models	Total cost ($)	Calculation time (second)		
		HPS	C&CG	BD
TDRC	942067.16	529.93	546.71	>1800
L_1	942134.13	538.31	541.09	>1800
SP [12]	942066.05	534.08	553.01	>1800
KL [20]	942072.42	538.44	553.44	>1800
Wasserstein [21]	942066.92	537.55	551.57	>1800

† The L_1-, KL- and Wasserstein-based methods correspond to different DRO models. The full names of these models are not provided in the table due to space limitations.

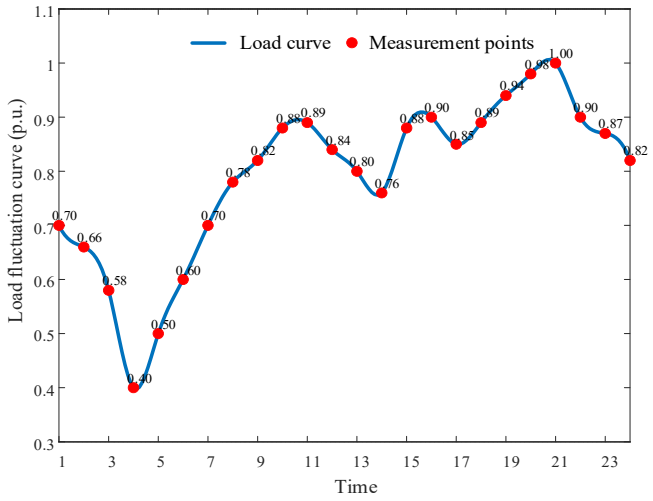

Fig. 9. 24-hour load fluctuation curve.

The results show that the proposed TDRC model achieves a lower total cost (i.e., $942,067.16) than the L_1-based and Wasserstein-based DRO methods, demonstrating superior economic performance. Although the total cost under the TDRC model is close to that obtained by the SP and Wasserstein-based DRO models, their practical applicability is limited because the SP method relies on assumed probability distributions and the Wasserstein approach involves high computational complexity. In addition, the EMS executes the HPS algorithm to solve the TDRC model in order to obtain the optimal dispatch decisions within 529.93 seconds, while data transmission and control instruction execution are completed in less than 1 second. Considering the day-ahead dispatch horizon, this computation time is acceptable. In addition, since real-time dispatch in power systems is typically updated every 15 minutes, the proposed HPS algorithm can be executed within this operational window to find the optimal solution, demonstrating the real-time applicability of the proposed TDRC approach for large-scale power systems. It is worth noting that the HPS algorithm converges faster than the C&CG method and avoids the non-convergence issue of BD under the same tolerance. It achieves convergence within approximately 530 seconds, while C&CG requires 540-550 seconds and BD fails to converge within 1800 seconds. These results confirm the superior computational efficiency and scalability of the proposed HPS algorithm for large-scale power system applications. In this paper, the wind power output forecasting code and the hardware-in-the-loop demonstration video of the proposed TDRC approach are publicly available and can be accessed online [38].

V. CONCLUSION AND FUTURE DIRECTION

This paper proposes a two-stage distributionally robust chance-constrained (TDRC) model for the unit commitment problem with wind power uncertainty. The TDRC model offers a comprehensive framework to address the inherent uncertainty of wind power and enhance the robustness of dispatch decisions in power systems. By constructing an ambiguity confidence set to manage wind power uncertainty and incorporating chance constraints to flexibly regulate wind power curtailment and load shedding levels, the model ensures system resilience against unpredictable variations in renewable energy generation. To obtain the optimal dispatch strategy, a hybrid parallel solution (HPS) algorithm is developed by integrating the advantages of BD and C&CG methods, thereby improving computational performance. The HPS algorithm decomposes the TDRC model into a master problem and multiple sub-problems that can be solved in parallel without relying on duality information, thus enhancing scalability and efficiency. The effectiveness and practical feasibility of the proposed TDRC approach are validated through extensive numerical simulations and further demonstrated on a cyber-physical power system dispatch platform, demonstrating its applicability in practical power system environments.

In the future work, several limitations of this paper will be addressed to enhance the practicality of the proposed model. More specifically, 1) the TDRC model only considers wind power uncertainty, while other stochastic factors such as load demand, photovoltaic generation, and market price fluctuations are not simultaneously considered. Further research will be conducted on incorporating multi-source uncertainties to provide a more comprehensive representation of stochastic characteristics in power systems; 2) the static and decision-independent ambiguity set may limit the TDRC model's ability to capture the interaction between dispatch decisions and uncertainty realisations. Developing a decision-dependent ambiguity set will better reflect this endogenous correlation between dispatch decisions and uncertainty realisations; 3) although the HPS algorithm improves computational efficiency, its scalability for larger-scale systems with high wind penetration still requires enhancement. Advanced decomposition and parallelisation methods will be further explored to improve the adaptability of the proposed model for large-scale real-world applications. In addition, future work will explore advanced machine learning approaches for predicting commitment decisions with high confidence and

fixing a subset of binary variables to further improve computational efficiency.

REFERENCES

[1] M. Du and X. Liu, "A Cyber-Secured Preventive Dispatch for Power Systems With High Wind Penetration," *IEEE Transactions on Power Systems,* vol. 39, no. 2, pp. 2398-2409, 2024.

[2] A. Saxena and R. Shankar, "An Interactive Operating Demand Response Approach for Hybrid Power Systems Integrating Renewable Energy Sources," *Protection and Control of Modern Power Systems,* vol. 9, no. 3, pp. 174-194, 2024.

[3] K. Qu, Y. Chen, S. Xie, X. Zheng, and J. Zhu, "Segmented Distributionally Robust Optimization for Real-Time Power Dispatch With Wind Uncertainty," *IEEE Transactions on Power Systems,* vol. 39, no. 2, pp. 2970-2983, 2024.

[4] D. Qiu, R. Zhang, Z. Zhou, J. Zhang, and X. Zhang, "Virtual‐physical power flow method for cyber‐physical power system contingency and vulnerability assessment," *IET Smart Grid,* vol. 7, no. 1, pp. 13-27, 2024.

[5] Z. Jiang, Q. S. Jia, and X. Guan, "A Computing Budget Allocation Method for Minimizing EV Charging Cost Using Uncertain Wind Power," *IEEE Transactions on Automation Science and Engineering,* vol. 18, no. 2, pp. 681-692, 2021.

[6] Z. Cai, C. Wei, S. Peng, and X. Wang, "Comprehensive Reliability Analysis of Fractional Frequency Offshore Wind Power Systems Considering Environmental Impact and Overall Structure: A Case Study in China," *Protection and Control of Modern Power Systems,* vol. 10, no. 1, pp. 64-75, 2025.

[7] S. Bhavsar, R. Pitchumani, J. Maack, I. Satkauskas, M. Reynolds, and W. Jones, "Stochastic economic dispatch of wind power under uncertainty using clustering-based extreme scenarios," *Electric Power Systems Research,* vol. 229, p. 110158, 2024.

[8] Y. Tang, Q. Zhai, and J. Zhao, "Multi-Stage Robust Economic Dispatch With Virtual Energy Storage and Renewables Based on a Single Level Model," *IEEE Transactions on Automation Science and Engineering,* vol. 21, no. 4, pp. 5490-5502, 2024.

[9] Y. Du, Y. Li, C. Duan, H. B. Gooi, and L. Jiang, "Adjustable Uncertainty Set Constrained Unit Commitment With Operation Risk Reduced Through Demand Response," *IEEE Transactions on Industrial Informatics,* vol. 17, no. 2, pp. 1154-1165, 2021.

[10] M. Qu, T. Ding, C. Mu, X. Zhang, K. Pan, and M. Shahidehpour, "Linearization Method for Large-Scale Hydro-Thermal Security-Constrained Unit Commitment," *IEEE Transactions on Automation Science and Engineering,* vol. 21, no. 2, pp. 1754-1766, 2024.

[11] J. Zhu, K. Zeng, J. Chen, W. Zhao, W. Liu, and W. Zhu, "Transfer-Based Approximate Dynamic Programming for Rolling Security-Constrained Unit Commitment with Uncertainties," *Protection and Control of Modern Power Systems,* vol. 9, no. 5, pp. 42-53, 2024.

[12] A. Fusco, D. Gioffrè, A. Francesco Castelli, C. Bovo, and E. Martelli, "A multi-stage stochastic programming model for the unit commitment of conventional and virtual power plants bidding in the day-ahead and ancillary services markets," *Applied Energy,* vol. 336, p. 120739, 2023.

[13] Y. Yang, W. Wu, B. Wang, and M. Li, "Chance-Constrained Economic Dispatch Considering Curtailment Strategy of Renewable Energy," *IEEE Transactions on Power Systems,* vol. 36, no. 6, pp. 5792-5802, 2021.

[14] Y. Ma, C. Liu, H. Yang, and D. Zhang, "Robust optimization of unit commitment with wind power considering composite flexibility constraints," *International Journal of Electrical Power & Energy Systems,* vol. 151, p. 109146, 2023.

[15] Y. Cho, T. Ishizaki, and J. I. Imura, "Three-Stage Robust Unit Commitment Considering Decreasing Uncertainty in Wind Power Forecasting," *IEEE Transactions on Industrial Informatics,* vol. 18, no. 2, pp. 796-806, 2022.

[16] X. Zheng, K. Qu, J. Lv, Z. Li, and B. Zeng, "Addressing the Conditional and Correlated Wind Power Forecast Errors in Unit Commitment by Distributionally Robust Optimization," *IEEE Transactions on Sustainable Energy,* vol. 12, no. 2, pp. 944-954, 2021.

[17] O. Yurdakul, F. Sivrikaya, and S. Albayrak, "A distributionally robust optimization approach to unit commitment in microgrids," in *2021 IEEE Power & Energy Society General Meeting (PESGM)*, 2021, pp. 1-5: IEEE.

[18] Q. Sha, W. Wang, and H. J. E. Wang, "A distributionally robust chance-constrained unit commitment with N-1 security and renewable generation," *Energies,* vol. 14, no. 18, p. 5618, 2021.

[19] J. Zhong *et al.*, "Optimal Operation of Energy Hub: An Integrated Model Combined Distributionally Robust Optimization Method With Stackelberg Game," *IEEE Transactions on Sustainable Energy,* vol. 14, no. 3, pp. 1835-1848, 2023.

[20] X. Feng, S. Lin, W. Liu, W. Liang, and M. Liu, "Distributionally Robust Optimal Dispatch of Offshore Wind Farm Cluster Connected by VSC-MTDC Considering Wind Speed Correlation," *CSEE Journal of Power and Energy Systems,* vol. 9, no. 3, pp. 1021-1035, 2023.

[21] X. Zheng *et al.*, "Day-ahead Network-constrained Unit Commitment Considering Distributional Robustness and Intraday Discreteness: A Sparse Solution Approach," *Journal of Modern Power Systems and Clean Energy,* vol. 11, no. 2, pp. 489-501, 2023.

[22] Z. Jin, K. Pan, L. Fan, and T. Ding, "Data-Driven Look-Ahead Unit Commitment Considering Forbidden Zones and Dynamic Ramping Rates," *IEEE Transactions on Industrial Informatics,* vol. 15, no. 6, pp. 3267-3276, 2019.

[23] A. Aharwar, R. Naresh, V. Sharma, and V. Kumar, "Unit commitment problem for transmission system, models and approaches: A review," *Electric Power Systems Research,* vol. 223, p. 109671, 2023.

[24] Q. Sun, Y. Zhang, Y. Zhou, J. Wang, Y. Zhao, and J. Wang, "Dynamic Regionalization for Unbalanced AC-DC Hybrid Distribution Systems With a Distributionally Robust Guarantee Against DG Uncertainty," *IEEE Transactions on Power Systems,* vol. 40, no. 2, pp. 1916-1930, 2025.

[25] L. Liu, W. Yang, S. Song, and Y. Zhang, "Distributionally Robust Chance-Constrained Line Planning for Railway Systems Under Passenger Demand Uncertainty," *IEEE Transactions on Automation Science and Engineering,* vol. 22, pp. 9457-9472, 2025.

[26] Z. Shi, H. Liang, and V. Dinavahi, "Data-driven distributionally robust chance-constrained unit commitment with uncertain wind power," *IEEE Access,* vol. 7, pp. 135087-135098, 2019.

[27] Z. Shi, H. Liang, S. Huang, and V. Dinavahi, "Distributionally Robust Chance-Constrained Energy Management for Islanded Microgrids," *IEEE Transactions on Smart Grid,* vol. 10, no. 2, pp. 2234-2244, 2019.

[28] Y. Ding, T. Morstyn, and M. D. McCulloch, "Distributionally robust joint chance-constrained optimization for networked microgrids considering contingencies and renewable uncertainty," *IEEE Transactions on Smart Grid,* vol. 13, no. 3, pp. 2467-2478, 2022.

[29] S. Fink, C. Mudd, K. Porter, and B. Morgenstern, "Wind Energy Curtailment Case Studies: May 2008 - May 2009," *NREL subcontract report, NREL/SR-550-46716,* 2009.

[30] Medina, Carlos, C. Ríos M. Ana, and Guadalupe González, "Transmission grids to foster high penetration of large-scale variable renewable energy sources–A review of challenges, problems, and solutions," *International Journal of Renewable Energy Research,* vol. 12, no. 1, pp. 146-169, 2022.

[31] T. Ding, Q. Yang, Y. Yang, C. Li, Z. Bie, and F. Blaabjerg, "A Data-Driven Stochastic Reactive Power Optimization Considering Uncertainties in Active Distribution Networks and Decomposition Method," *IEEE Transactions on Smart Grid,* vol. 9, no. 5, pp. 4994-5004, 2018.

[32] S. Shokrzadeh, M. J. Jozani, and E. Bibeau, "Wind Turbine Power Curve Modeling Using Advanced Parametric and Nonparametric Methods," *IEEE Transactions on Sustainable Energy,* vol. 5, no. 4, pp. 1262-1269, 2014.

[33] A. Ahmadpour and S. Gholami Farkoush, "Gaussian models for probabilistic and deterministic Wind Power Prediction: Wind farm and regional," *International Journal of Hydrogen Energy,* vol. 45, no. 51, pp. 27779-27791, 2020.

[34] W. Wei, N. Li, J. Wang, and S. Mei, "Estimating the Probability of Infeasible Real-Time Dispatch Without Exact Distributions of Stochastic Wind Generations," *IEEE Transactions on Power Systems,* vol. 31, no. 6, pp. 5022-5032, 2016.

[35] F. Pecci and J. D. Jenkins, "Regularized Benders Decomposition for High Performance Capacity Expansion Models," *IEEE Transactions on Power Systems,* vol. 40, no. 4, pp. 3105-3116, 2025.

[36] J. Feng, Z. Ren, and W. Li, "Soft Actor-Critic Combined With Logic-Based Benders Decomposition Algorithm for Monthly Security Constrained Unit Commitment Under Wind Power Uncertainty," *IEEE Transactions on Power Systems,* vol. 40, no. 6, pp. 4784-4796, 2025.

[37] B. A. Studio, "State Grid AI Innovation Competition: Intelligent Scheduling of Power Grid Operation Organization," [Online] *Available: https://aistudio.baidu.com/competition/detail/111/0/introduction,* 2021.

[38] T-ASE-2025-2438, "IEEE-TASE," GitHub, 2025. [Online]. Available: *https://github.com/T-ASE-2025-2438/IEEE-TASE*.

Min Du (Member, IEEE) received the B.Sc. degree from the School of Electrical and Information Engineering, Wuhan Institute of Technology, Wuhan, China, in 2016, and the M.Sc. and Ph.D. degrees from the College of Electrical and Information Engineering, Hunan University, Changsha, China, in 2019 and 2023, respectively. He is currently a Postdoctoral Research Associate with The University of Sheffield, U.K. His research interests include cyber-physical power systems, cybersecurity, and resilience.

Xin Zhang (Senior Member, IEEE) received the B.Eng. degree in automation from Shandong University, China, in 2007, and the M.Sc. and Ph.D. degrees in electrical power engineering from The University of Manchester, U.K., in 2007 and 2010, respectively. He is currently a Professor of control and power systems with the School of Electrical and Electronic Engineering, University of Sheffield, U.K. He was with National Grid Electricity System Operator, where he worked on the real-time power system operation at the Electricity National Control Centre, Wokingham, U.K. His research interests include cyber-physical power system security and resilience, power system operation, and grid-integrated transport electrification. He was the recipient of the U.K. Research and Innovation Future Leaders Fellowship In 2022. He serves as an Associate Editor for IEEE Transactions on Smart Grid and IEEE Power Engineering Letters.

Jinning Zhang (Member, IEEE) received the B.S. degree in vehicle engineering from Nanjing University of Aeronautics and Astronautics, Nanjing, China, in 2018, and the M.Sc. and Ph.D. degrees in aerospace propulsion from Cranfield University, Cranfield, U.K., in 2019 and 2022, respectively. She is currently a Lecturer (Assistant Professor) in aerospace and computational engineering with the University of Leicester, Leicester, U.K. Her research interests include energy management strategies and integrated control system design for aerospace propulsion, artificial intelligence for transport and energy systems, and transportation-energy nexus.

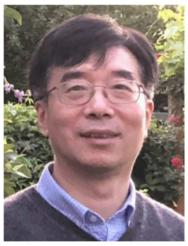

Zidong Wang (Fellow, IEEE) received the B.Sc. degree in mathematics in 1986 from Suzhou University, Suzhou, China, the M.Sc. degree in applied mathematics and the Ph.D. degree in electrical engineering from Nanjing University of Science and Technology, Nanjing, China, in 1990 and 1994, respectively. He is currently Professor of Dynamical Systems and Computing in the Department of Computer Science at Brunel University of London, U.K. From 1990 to 2002, he held teaching and research appointments in universities in China, Germany, and the U.K. Prof. Wang's research interests include dynamical systems, signal processing, bioinformatics, control theory, and their applications. He has published a number of papers in international journals. He is a recipient of the Alexander von Humboldt Research Fellowship (Germany), the JSPS Research Fellowship (Japan), and the William Mong Visiting Research Fellowship (Hong Kong).

Prof. Wang serves or has served as Editor-in-Chief of the International Journal of Systems Science, Neurocomputing, and Systems Science & Control Engineering, and as an Associate Editor for 12 international journals, including IEEE Transactions on Automatic Control, IEEE Transactions on Control Systems Technology, IEEE Transactions on Neural Networks, IEEE Transactions on Signal Processing, and IEEE Transactions on Systems, Man, and Cybernetics-Part C. He is a Member of the Academia Europaea, a Member of the European Academy of Sciences and Arts, an Academician of the International Academy for Systems and Cybernetic Sciences, a Fellow of the IEEE, a Fellow of the Royal Statistical Society, and a member of the program committee for many international conferences.

Vladimir Terzija (M'95-SM'00-F'16) was born in Donji Baraci (former Yugoslavia). He received the Dipl.-Ing., M.Sc., and Ph.D. degrees in electrical engineering from the University of Belgrade, Belgrade, Serbia, in 1988, 1993, and 1997, respectively. He is a Professor of Energy Systems & Networks at Newcastle University, U.K. He is also a Distinguished Visiting Professor at Shandong and Tsinghua Universities, China, as well as a Guest Professor at the University of Belgrade, Chongqing University and the Technical University of Munich, Germany. From 2021 to 2023, he was a Full Professor at Skoltech, Russian Federation. From 2006 to 2020, he held the EPSRC Chair Professorship at the University of Manchester, U.K. From 2000 to 2006, he was a Senior Specialist in switchgear and distribution automation at ABB, Ratingen, Germany. From 1997 to 1999, he was an Associate Professor at the University of Belgrade, Belgrade, Serbia. His current research interests include smart grid applications; wide-area monitoring, protection and control; multi-energy systems; big data analytics; and applications of complexity science in power systems. From 2015 to 2025, he served as Editor-in-Chief of the International Journal of Electrical Power and Energy Systems. He is a Humboldt Fellow and a recipient of the National Friendship Award of China.